Article

Effect of Corrosion-Induced Structural Degradation on the Ultimate Strength of a High-Tensile-Steel Ship Hull

Nikola Momčilović [1,*], Nemanja Ilić [1], Milan Kalajdžić [1], Špiro Ivošević [2] and Ana Petrović [1]

1   Faculty of Mechanical Engineering, University of Belgrade, 11120 Belgrade, Serbia;
    d46-2021@studenti.mas.bg.ac.rs (N.I.)
2   Faculty of Maritime Studies Kotor, University of Montenegro, 85331 Kotor, Montenegro
*   Correspondence: nmomcilovic@mas.bg.ac.rs

Abstract: Standard structural assessments of ship hulls include the evaluation of the elastic structural response. Elastic analysis neglects extreme and unpredicted loadings, which can produce catastrophic outcomes, such as the loss of the ship's ultimate strength. Moreover, hull elements are considered unaffected by age-related degradation. Therefore, this study models and quantifies the effect of corrosion-induced structural degradation on the ultimate strength of a high-tensile-steel (HTS) cargo ship using progressive collapse and nonlinear finite element methods. Uniform and pitting corrosion are modeled through selected scenarios, which hull elements might encounter during exploitation, producing a total of 148 calculation models. The findings show that corrosion-induced degradation can significantly decrease the ultimate strength of the hull (up to 30% for the most severe scenarios assessed). Furthermore, ultimate strength decreases almost proportionally to the amount of wastage considered. It was found that stiffener corrosion has a significant effect on the total ultimate strength. This study's aim is to emphasize the vast importance of including ultimate strength along with ageing effects in industry-standard structural assessments of large HTS ship structures, designed to last for several decades whilst exposed to excessive and unpredicted bending moments.

Keywords: ultimate strength; hull girder; corrosion wastage; progressive collapse; NLFEM

1. Introduction

In practice, almost all ship structural assessments are based on the linear–elastic behavior of the material. Maximum stress is derived from service loadings and then evaluated with respect to the maximum allowable stress (i.e., the allowable stress criterion), which is the share of the yield stress of the material [1,2]. This share, which acts as a safety margin, is defined by classification societies' rules and regulations for ships [3,4]. This traditional approach is generally believed to ensure the structural integrity of the ship.

However, a ship's resilience to extreme or once-in-a-lifetime scenarios is often neglected in structural assessments. As ships are designed to last for several decades, they are prone to experiencing extreme events, unpredicted in the design phase, that can lead to catastrophic structural failures, such as the loss of the ship's ability to carry loads, labelled as the loss of ultimate capacity (i.e., ultimate strength), which can consequently cause the ship to break in two and lead to the loss of the hull [5]. This can occur due to large bow waves, grounding, overloading, combined events, etc. In addition, when excessive loadings are coupled with the degradation of hull elements due to ageing, ultimate strength loss can be even more accelerated; see the cases of the MSC Comfort [6] and the MV Arvin [7] and the chronology of a structural collapse in [8]. Ultimate strength assessments differ from traditional ones as they take into account nonlinear effects on both material and geometry. Moreover, classification societies acknowledge these phenomena. Following the adoption of Common Structural Rules for Bulk Carriers (CSR-BC) and Oil Tankers (CSR-BC) by the International Association of Classification Societies (IACS) in 2005 and the International

Maritime Organization's (IMO) goal-based standards established in 2010 [9], the IACS has pursued the development of joint rules incorporating ultimate strength assessments for these two ship types. CSR-BS and CSR-OT were harmonized in [10], while the most recent IACS rules were published in [11]. Other classification societies have also incorporated ultimate strength assessments [3,4]. Two methods were emphasized by the IACS [11]: progressive collapse analysis (PCA) and the nonlinear finite element method (NLFEM). In addition, the procedures and practices of and guidance for ultimate strength assessments of ship structures are systematized in [12].

Furthermore, during the preliminary design phase, ship structural assessments are performed almost entirely using as-built scantlings of the new ship. When ship platings experience reduced thickness over time, classification society standards prescribe allowed corrosion wastage (in general, up to 20–25% of the original thickness) [13,14]. If the allowed corrosion wastage is exceeded, then this particular plating is renewed. The importance of integrating ageing phenomena into ultimate strength calculations for ships is underlined in [15]. Most investigations include thickness reductions but do not take into account changes in the mechanical properties of the material. On the other hand, Ref. [16] proposed a methodology, which implicitly incorporated changes in material properties by deriving the corrosion factor. Nevertheless, in the past decade, studies regarding the ultimate strength assessment of cargo ships have been carried out, taking into account numerous conditions: the intact state, corrosion, damage, grounding, cyclic loads, etc. PCA is applied to five cargo ship structures in [17]. The effect of NLFEM-derived load-end shortening curves on PCA results is explored in [18]. PCA is used to evaluate the ultimate strength of ten ships while assessing multiple variations such as discretization and initial deflection of plates in [19]. PCA and NLFEM are applied to compare the ultimate strengths of a container ship and a tanker [20,21], respectively, taking into account damage and the intact condition. Furthermore, Ref. [22] uses the NLFEM to estimate ultimate strength under combined wave loads. Cyclic loads are also considered in [23], where their effect is compared to the effect of monotonic loading, concluding that those loadings produce negligible differences in terms of ultimate strength results. In addition, an analysis of methods for the evaluation of the ultimate strength of a grounded ship is assessed in [24,25].

When it comes to corrosion only, it is modeled in [26] using the PCA method. Uniform and pitting corrosion models are calculated for up to 25 years for an FPSO ship, showing that both types of corrosion degradation produce similar outcomes in terms of ultimate strength reductions. A methodology for ultimate strength reassessment based on an updated corrosion time-variant model is given in [27]. Furthermore, Ref. [28] explores the effect of corrosion on the ultimate strength of VLCC using PCA and the probabilistic estimation of corrosion degradation, whereas [29] considers local corrosion's impact on the ultimate strength of hull girders using IACS PCA. A corrosion wastage model for the ultimate strength of bulk carriers and tankers is presented in [30] using a probabilistic approach. In [31], the authors quantify the difference between an intact and a severely corroded bulk carrier affected by uniform and pitting corrosion for a specific diminution, concluding that the ultimate strength can be reduced by up to 30%.

In order to incorporate corrosion-induced degradation into methods for the assessment of the ultimate strength of hull girders, numerous studies have been performed on the level of stiffened plates. In [32], pitting is modeled in PCA based on the authors' previous research on a unified formulation for pitted platings [33,34]. The former study shows that in a wide range of the investigated cases, pitting-induced volume loss can lead to a more than 15% reduction in ultimate strength. Similar to the latter two studies, in [35], the authors calculate ultimate strength on based the level of corroded platings using extensive numerical assessments. Pitting corrosion's effect on the ultimate strength of stiffened panels based on pit depth and quantity is also examined in [36]. In addition to determining the level of corrosion wastage, it is shown that a lot of uncertainties govern the ultimate strength of stiffened panels and, thus, that of a hull girder. To acknowledge this, the impact of uncertainties on the ultimate strength of a stiffened plate is evaluated in [37] using a

probabilistic approach, whereas purely geometrical uncertainties are considered in [38]. Finally, a review of studies dealing with intact ultimate strength is given in [39], while a review on ageing and damage effects on the ultimate strength of ships is presented in [40].

To conclude, numerous studies have addressed the ultimate strength of ships affected by service factors, such as grounding, collision, and corrosion. In particular, the effect of corrosion on the ultimate strength of cargo ships is examined using various non-unified methodologies. However, the literature on this topic remains unharmonized and calls for novel approaches and data regarding the effects of corrosion on ships. Whilst the abovementioned studies have been mostly focused on larger cargo ships due to their susceptibility to longitudinal strength issues, this study's aim is to enhance the understanding of corrosion-induced degradation and its effect on the ultimate strength of a smaller cargo ship built purely of a high-tensile steel (HTS). HTS is used to allow for larger hull stresses, thereby reducing the steel weight. However, due to its high cost, HTS is generally used in critical areas. Nonetheless, it is very rare to encounter a ship constructed entirely of HTS. The ship is built according to the class of the American Bureau of Shipping (ABS). The bulk carrier is chosen because this type represents the largest share of the merchant ships, accounting for 34% [41]. This fleet also experiences an annual growth of 3.61% by deadweight [42]. Therefore, for the selected ship, scenarios of both uniform and pitting corrosion are investigated in terms of their effects on reducing the ship's ultimate strength. The novel approach presented in [32] is adopted here for the purpose of analysis. Note that an actual ship structure was presented in [31]; yet, that study included only six calculation models. On the contrary, this study presents an additional 148 calculation models based on various corrosion scenarios that may affect the hull, with the objective of determining actual reductions in ultimate strength due to corrosion.

2. Case Study Ship

The case study ship is represented by a handysize bulk carrier hull, which includes an open cross-section comprising double-bottom and double-side structures (see Figure 1). The ship's overall length is 180 m, the breadth is 30 m, and the height is 14.7 m (see Table 1). The hull is longitudinally framed, meaning that all secondary stiffeners consist of longitudinals. Almost all longitudinals are bulb profiles, except for five deck longitudinals, which consist of flat bars. Most of the longitudinals are spaced 800 mm apart. The primary bottom longitudinal structure consists of a central girder and four pairs of the bottom-side girders connecting the bottom and inner bottom platings. The double-side structure includes three side girders, while the upper one acts as a bottom of the wing tank (i.e., top tank). Deck and below-deck structures have one deck girder cutting through the wing tanks. The hatch coaming is 2.05 m in height and includes a strong stiffener at the top. The web frame sections are spaced 2.4 m apart. The main material of the hull is AH32. In addition, even stronger material (AH36) was used for specific parts of the ship, namely, all inner-bottom and the two downmost inner-side longitudinals (the strengthening plates directly exposed to the grabber during loading/unloading operations), deck, below deck, hatch coaming plates and longitudinals (due to high normal stresses in the most distanced elements from neutral axis of the cross-section). The minimal requirements with which HTS must comply for bulk carriers are defined in [43].

Table 1. Ship particulars and material data.

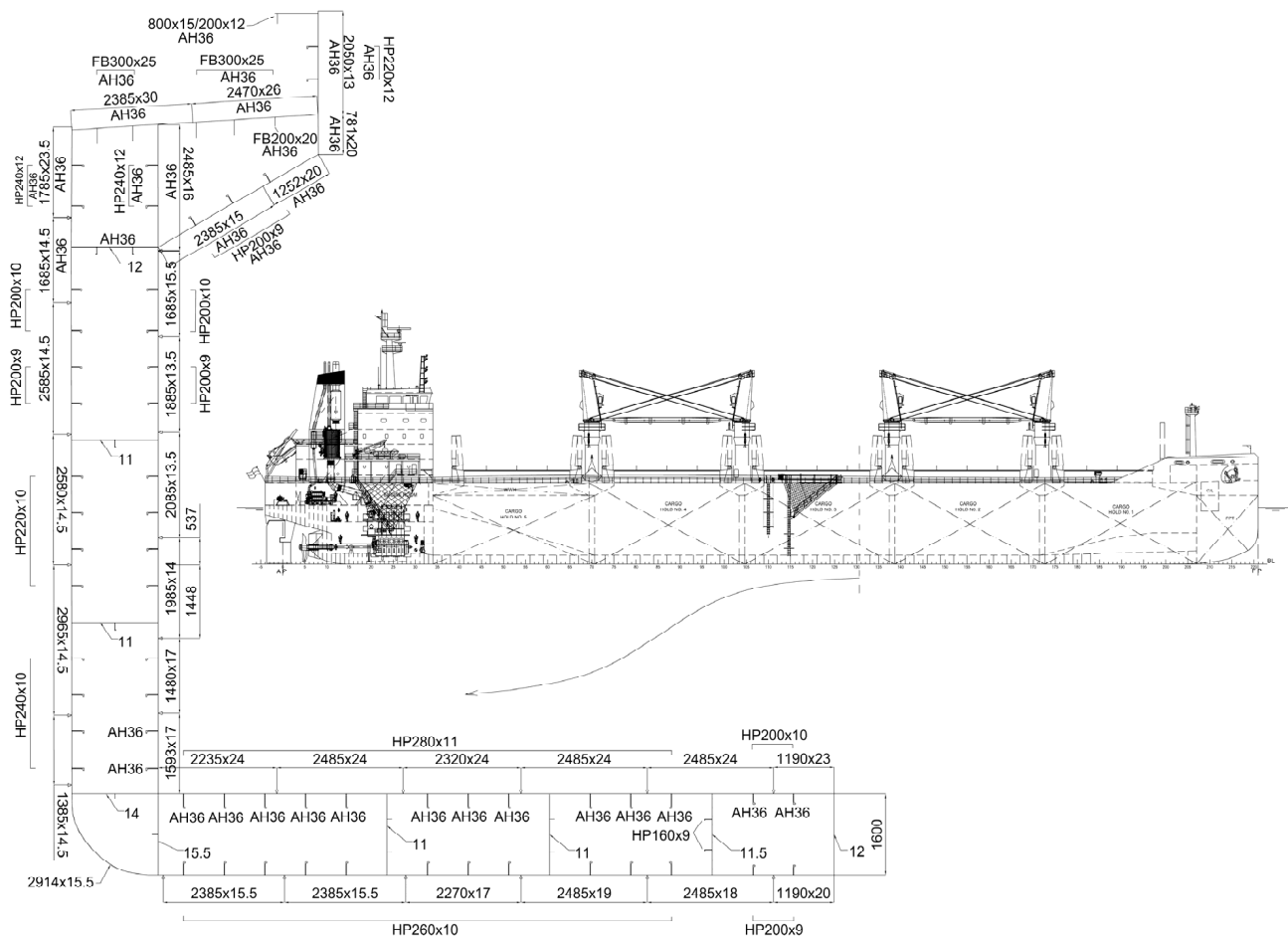| Item	Data
Length overall × breadth × height	180 m × 30 m × 14.70 m
Maximum draught	10.30 m
Material modulus of elasticity (AH32 and AH 36)	206,000 N/mm^2
Material Poisson's ratio (AH32 and AH 36)	0.30
Material yield strengths for AH32 and AH36	315 N/mm^2 (AH32) and 355 N/mm^2 (AH36)

Figure 1. Cross-section of the midship and lateral plan of the ship.

3. Methodology

The methodology includes two of the most contemporary methods used for ultimate strength assessments of ship hulls (PCA and NLFEM), according to the best practice and recommendations given by the classification societies [3,4,11], literature [1,2,5], ultimate Strength Committee of the International Ship Structure Congress (ISSC) [12,25], and the majority of studies reviewed in the Introduction section. Furthermore, the corrosion inputs are modeled using the most recent findings and formulas from the literature [32–34].

3.1. PCA

PCA originated from the Smith method [44]. Currently, it forms a basis of an incremental–iterative method given in the IACS' Common Structural Rules for Bulk Carriers and Oil Tankers (CSR) [11], where the detailed procedure for calculating the ultimate strength is described and, thus, employed here. It consists of the following steps, adjusted for the case study ship hull:

1. Cross-section of the hull midship is divided into segments of the following three types, as in Figure 2a: plates, stiffener with attached plate, and hard corner. The cross-section and segments span between transverse framing sections (floors, web frames, deck transverses), which are 2.4 m apart.

2. Based on segment's material and structure, different stress–strain curve is derived for each of the segments: elastic-perfectly plastic curve for tension, and several modes of buckling-governed curves in compression. Only hard corner segments have an elastic-perfectly plastic behavior both in compression and tension, due to their rigidity

and the assumption that they will firstly yield and then buckle (see Figure 2b and Table 2).

3. An incremental–iterative curvature (χ) is imposed on the midship cross-section, as in Figure 2c, meaning that in each step, the curvature increment is increasing while producing strain (ε_i) and consequent stress (σ_i) on each of the cross-section segments (n—total number of segments). Moreover, in each of the curvature increasing increment steps ($\Delta\chi$), a total equilibrium of axial forces has to be established according to Equation (1), based on the sum of the cross-section (A_i) and normal stress (σ_i) product of each of the segments. Then, the change, i.e., the new position of neutral axis of the cross-section (z_n), has to be calculated, see Equation (2), followed by the strain in Equation (3), which uses the position of novel neutral axis (z_n), distance of each of the segments (z_i), and the product $A_i\sigma_i$. Consequently, a bending moment (M) imposed on the structure can be determined using Equation (4).
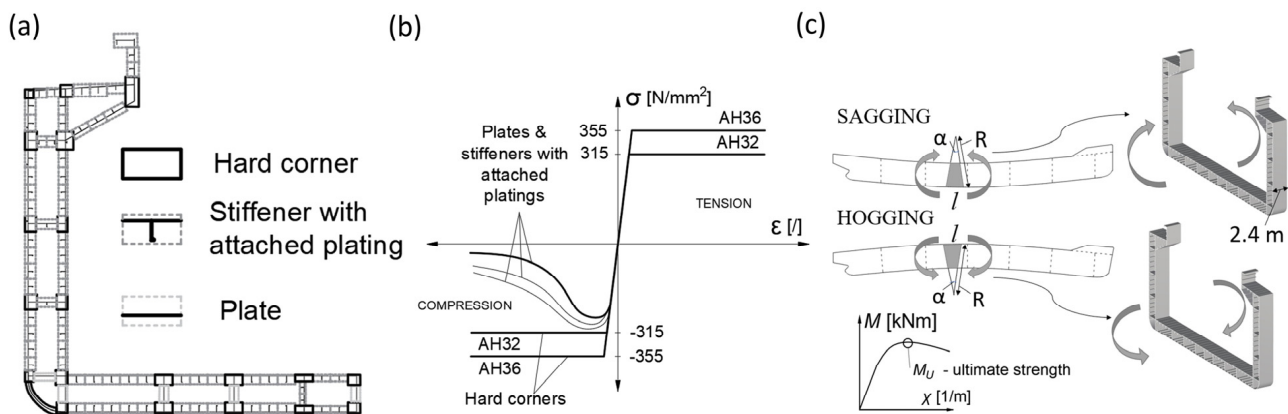

Figure 2. (**a**) Cross-section divided into segments, (**b**) stress–strain curves for segments, (**c**) imposing a curvature and a bending moment–curvature diagram.

It is assumed that the vertical plane of the cross-section remains undeformed (planar) after the imposition of curvature. The last (third) step is repeated after every increment of the curvature, until the total bending moment (M) reaches the point from which the slope of the bending moment–curvature diagram becomes negative (Figure 2c). This bending moment is called the ultimate bending moment, i.e., ultimate strength of the hull (M_U).

Table 2. Failure modes.

Segment	Failure Mode	Stress–Strain Curve Formulations
Plates	Plate buckling	Formulations applied are completely defined in IACS Appendix 2—Hull girder ultimate capacity, in 2.3.8 [11]
Stiffener with attached plate	– Beam column buckling – Torsional buckling – Web local buckling of flanged profiles – Web local buckling of flat bars	Formulations applied are completely defined in IACS, Appendix 2—Hull girder ultimate capacity [11], in: 2.3.4—for beam column buckling 2.3.5—for torsional buckling 2.3.6—for web local buckling of flanged profiles 2.3.7—for web local buckling of flat bars
Hard corner	Elastic-plastic collapse	Formulations applied are completely defined in IACS Appendix 2—Hull girder ultimate capacity, in 2.3.3 [11]; see stress–strain curve for hard corners in Figure 2b

The limitations of the method consist of neglecting the interaction between segments, as well as the simplified assumptions described here. The method considers only the axial compression of the segments, which is, indeed, the dominant feature but not the only one. The potential rotation of the neutral axis is not considered. Moreover, initial imperfections (initial deflections and residual stresses) are excluded from direct calculations. However, regulations treat them as a safety factor in the later stages of assessments when checking the ultimate bending moment.

$$\int_{i=0}^{n} A_i\sigma_i = 0 \tag{1}$$

$$z_n = \frac{\sum_{i=0}^{n} A_i\sigma_i}{\sum_{i=0}^{n} A_i} \tag{2}$$

$$\varepsilon_i = \chi(z_i - z_n) \tag{3}$$

$$M = \sum_{i=1}^{n} A_i\sigma_i|z_i - z_n| \tag{4}$$

3.2. NLFEM

NLFEM requires significantly more computational time, and, thus, it is used here to act as a confirmation of the PCA results. The method is described in the systematically presented literature on this topic [1,2,5,25]. The mesh is refined to facilitate the buckling modes and to follow the ISSC recommendations [18,25]. The mesh consists of four-node plate thin-shell elements. The distance between the secondary stiffeners is divided by 10 elements, whilst the stiffeners' height consists of 6 elements (Figure 3). The total number of elements in the model is 76,416. A nonlinear analysis is included through the consideration of nonlinear geometry (large deformations) and nonlinear material behavior. The model is constrained in one node (node no. 1 in Figure 3) located at the symmetry line and vertically distanced by z_n = 5824.7 mm from the baseline, as this is the initial position of the neutral axis. The second node (no. 2) has the same vertical location but on the other end of the model. Nodes are connected to all corresponding nodes from their planes, via multiple rigid constraints, in order to avoid end plane deformations. All six degrees of freedom (DoF) are disabled for node no. 1 (three translations and three rotations). Node no. 2 is used for the imposition of the curvature, which produces the rotation α (see Figure 2c and Equation (5)). Consequently, the bending moment reaction in node 1 is recorded.
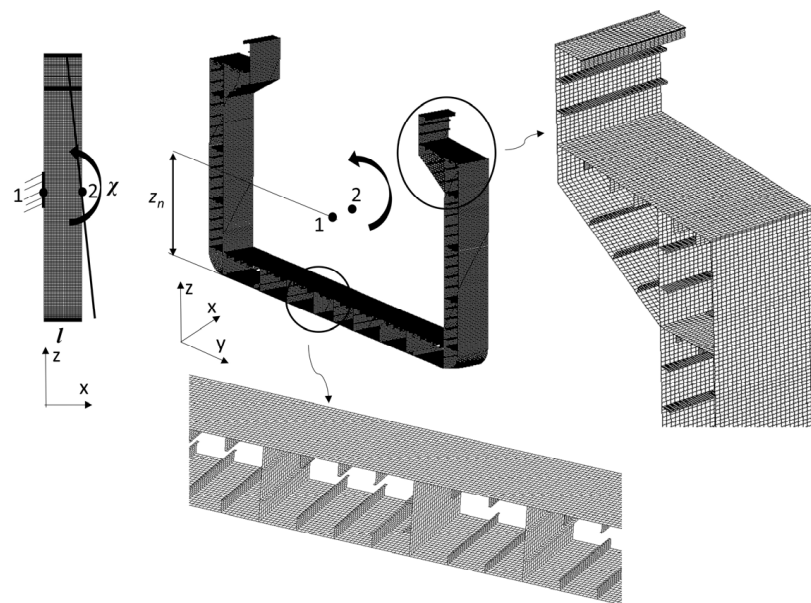

Figure 3. NLFEM model.

A limitation of this method is the large computational time required for analysis, neglecting residual stresses and initial imperfections, and considering only the vertical bending moment. However, contrary to PCA, NLFEM includes the effect of interactions between segments. Material nonlinearities are modeled as perfectly plastic, according to IACS recommendations [11].

$$\alpha = \chi l \tag{5}$$

3.3. Corrosion

Two types of corrosion are considered: uniform and pitting. Both are integrated within the PCA method. However, in NLFEM, only uniform corrosion is assessed. In addition, both methods use presumed corrosion degradation and not time-variant degradation.

Uniform corrosion is modeled by including the corrosion wastage (thickness reduction Δt) as a share of the original thickness of element t (Figure 4a) to obtain the new reduced thickness t_{corr}, see Equation (6). Decreased thickness t_{corr} increases the stiffener with the attached plate slenderness ratio λ according to Equation (7), where L is the length of the stiffeners, σ_y is the yield stress of the segment material, E is the modulus of elasticity, and r is the radius of gyration, depending on the cross-sectional moment of inertia (I) and area (A), see Equation (8). So, the reduced thickness directly influences the radius of gyration through reductions in the cross-sectional properties of a segment. Moreover, by reducing the thickness, the slenderness ratio of the plate segments (β) is also increased according to Equation (9) through the reduced thickness t_{corr}. Here, b stands for the width of the plate. Thus, the ultimate strength formulation for segments ϕ_{ult} (for compressive, i.e., buckling failure modes) from IACS, see [12] and Table 2, is updated with the new slenderness ratio for uniformly corroded segments, see Equation (10).

$$t_{corr} = t(1 - \Delta t / t) \tag{6}$$

$$\lambda = \frac{L}{\pi r}\sqrt{\frac{\sigma_Y}{E}} \tag{7}$$

$$r = \sqrt{I/A} \tag{8}$$

$$\beta = \frac{b}{t}\sqrt{\frac{\sigma_Y}{E}} \tag{9}$$

$$\phi_{ult}(\beta) = \left\{ \begin{array}{l} 1 \text{ if } \beta \leq 1.25 \\ \frac{2.25}{\beta} - \frac{1.25}{\beta^2} \text{ if } \beta > 1.25 \end{array} \right\} \tag{10}$$
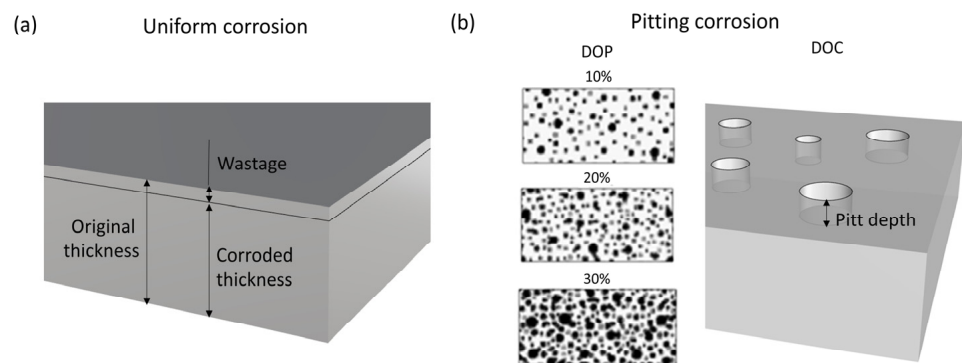

Figure 4. (**a**) Uniform corrosion; (**b**) pitting corrosion.

On the other hand, pitting corrosion is modeled according to a novel approach labelled as the Modified Incremental–Iterative Method proposed in [32], in which the PCA method is updated in the following ways:

1. The pitting intensity degree (DOP) and corrosion intensity degree (DOC) of the affected zone are assumed. DOP is the share of pits in the total element surface area, while DOC is the share of thickness wastage depth in pits (Figure 4b).
2. The total volume of element wastage due to pits is calculated using Equation (11), and the equivalent thickness (average reduced thickness due to pitting) t_{corr} of the pit-affected element is calculated using total volume loss ΔV and reduced thickness from Equation (12).
3. Equivalent (increased) slenderness ratio equations are updated with the thickness from Equation (12), see Equations (7)–(9).
4. The standard ultimate strength formula is updated with an equivalent slenderness ratio of the pit-affected element, as in Equation (10).
5. The ultimate strength of the pit-affected element is calculated according to Equation (13). This formulation is proposed in [32] for pitted elements and evaluated on a series of analyses for segments, which can be found in [33,34]. Therefore, here, it is used as such for the purpose of evaluating the complete ship hull.

$$\Delta V = DOP \cdot DOC \tag{11}$$

$$t_{corr} = t(1 - \Delta V) \tag{12}$$

$$\phi_u, \ pit = \phi_u(\ \beta)[1 - 1.5 \ DOP \ DOC] \tag{13}$$

3.4. Scenarios

In the first stage, the ultimate strength of the hull girder with original thicknesses is assessed (intact hull), using NLFEM for sagging and hogging, to complement the PCA results for the same conditions as delivered in [31]. However, in this study, both PCA and NLFEM are applied for uniform corrosion scenarios, while PCA is applied for pitting corrosion scenarios. Uniform corrosion is considered through the three corrosion wastages: 10%, 20%, and 25%. It produced three uniform corrosion models for sagging and three for hogging. In addition, pitting corrosion is modeled by varying five DOP (5%, 10%, 20%, 30%, 40%) and three DOC (10%, 20%, 40%) inputs to form a total of 15 models of volume losses ($\Delta V = DOP \times DOC$) for sagging and 15 for hogging (30 in total for one case) (see Tables 3 and 4 and Figure 5). However, some of those combinations give the same volume loss, so the total independent variations in ΔV are 9 for each bending response (sagging and hogging) with the following percentages: 0.5%, 1%, 2%, 3%, 4%, 6%, 8%, 12%, and 16%. All the abovementioned variations in material diminutions are included in the total of five cases of a corrosion-degraded hull. These cases are selected based on previous research performed by [32], although slightly modified here; see Figure 5 for an illustration and explanation regarding which elements were considered as corroded. Case I is considered as a severe corrosion-impacted hull and acts as a benchmark for further analyses. Case II examines the effects of stiffener exclusion as the corrosion is not accounted for. The following cases are more likely to be experienced on this type of ship. The total number of calculation models established in this study is 148, and an additional 6 were utilized in [31] and were included here to complement the findings presented in this study, see Table 4. Table values colored in red represent calculation models already given in [31] by using PCA for the intact condition, case I (the same as case I here but performed there for only 25% wastage for uniform, and 16% of volume loss for pitting corrosion).

Table 3. Volume losses based on combinations of DOP and DOC.

DOP=	5%	10%	20%	30%	40%
DOC = 10%	0.5%	1%	2%	3%	4%
DOC = 20%	1%	2%	4%	6%	8%
DOC = 40%	2%	4%	8%	12%	16%

Table 4. Number of calculation models.

Intact Hull	PCA		NLFEM	
	Sagg.	Hogg.	Sagg.	Hogg.
	1	1	1	1

Corrosion-Degraded Hull	Uniform Corrosion				Pitting Corrosion			
	PCA		NLFEM		PCA		NLFEM	
	Sagg.	Hogg.	Sagg.	Hogg.	Sagg.	Hogg.	Sagg.	Hogg.
Case I	2 + 1	2 + 1	3	3	8 + 1	8 + 1	0	0
Case II	3	3	3	3	9	9	0	0
Case III	3	3	3	3	9	9	0	0
Case IV	3	3	3	3	9	9	0	0
Case V	3	3	3	3	9	9	0	0
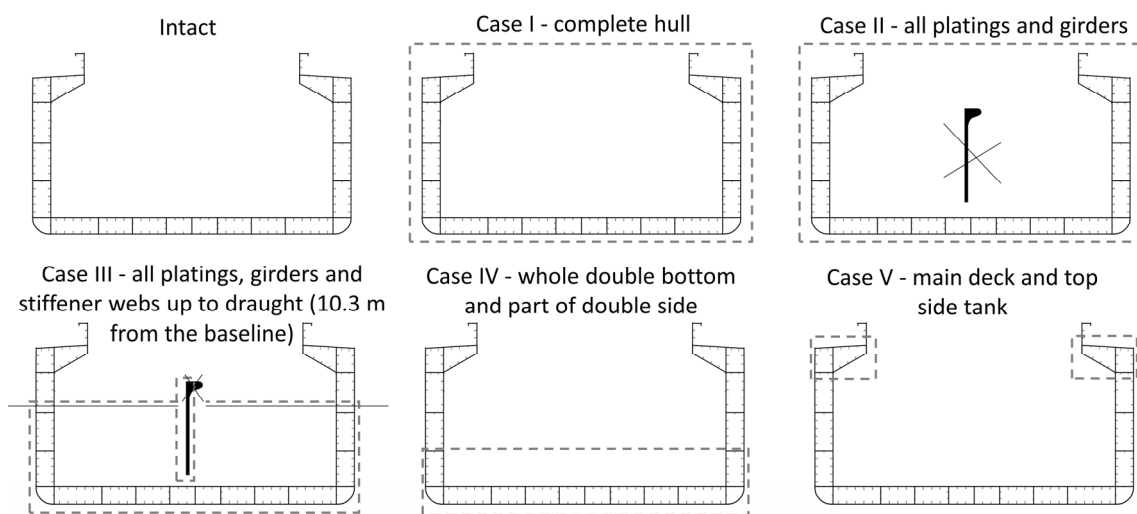
Figure 5. Corrosion cases.

The main limitation of this approach lays in the fact that corrosion scenarios are presumed and not actually obtained. This is due to the lack of harmonized results found in the literature with respect to time-dependent corrosion. These studies do exist [13,45,46]. However, the data are dispersed and are highly influenced by the ship navigation conditions, operation, coating duration, loading/unloading conditions, selection of ship types, etc. This is why it is neglected here. Therefore, the aim of the approach presented in this study is to showcase the methodology for ultimate strength assessment based on the known corrosion rate, independently of the ship service time for which the corrosion is recorded.

4. Results and Discussion

Uniform and pitting corrosion effects on ultimate strength are given separately. Figures 6–10 present the effect of uniform input variations on ultimate strength, along with the results for the intact condition, performed using PCA and NLFEM. Figures 11–15 show the effects of pitting corrosion input variations on ultimate strength, also compared to intact condition values, calculated using PCA. Figure 16 summarizes the findings, providing 3D plots for a more insightful illustration of the general tendencies extracted from the PCA approach. The results are represented through the bending moment–curvature diagrams for sagging and hogging while also accounting for the volume loss. Moreover, the pitting corrosion results of the ultimate strengths are broken down into DOP and DOC variables.
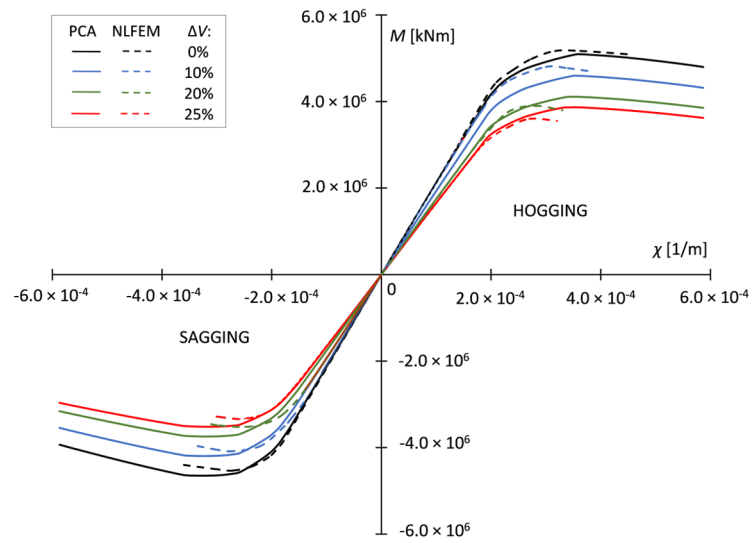
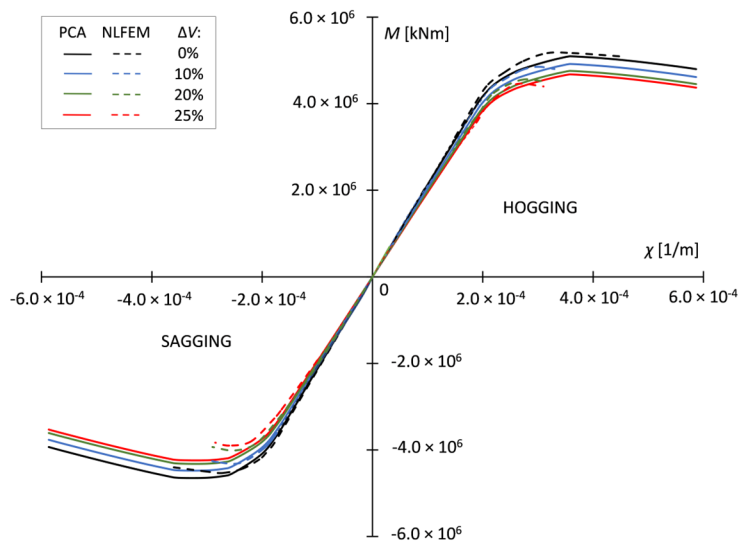**Figure 6.** Case I—intact and uniform corrosion-affected hull: bending moment vs. curvature.

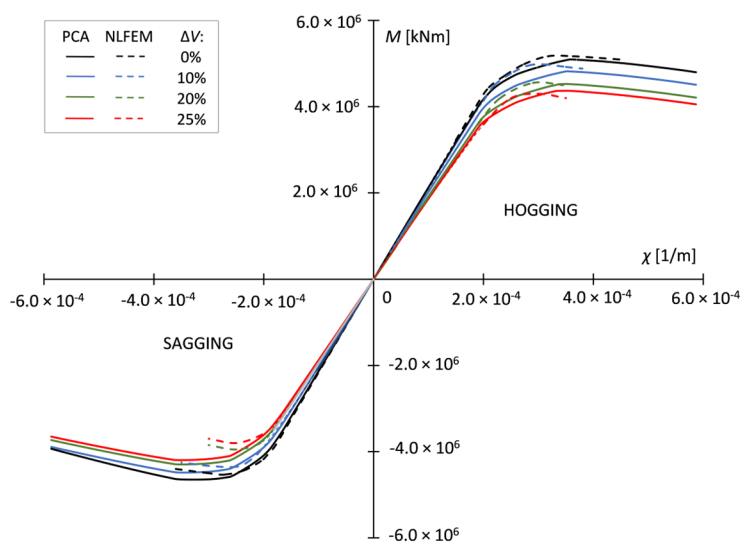**Figure 7.** Case II—intact and uniform corrosion-affected hull: bending moment vs. curvature.

Figure 8. Case III—intact and uniform corrosion-affected hull: bending moment vs. curvature.
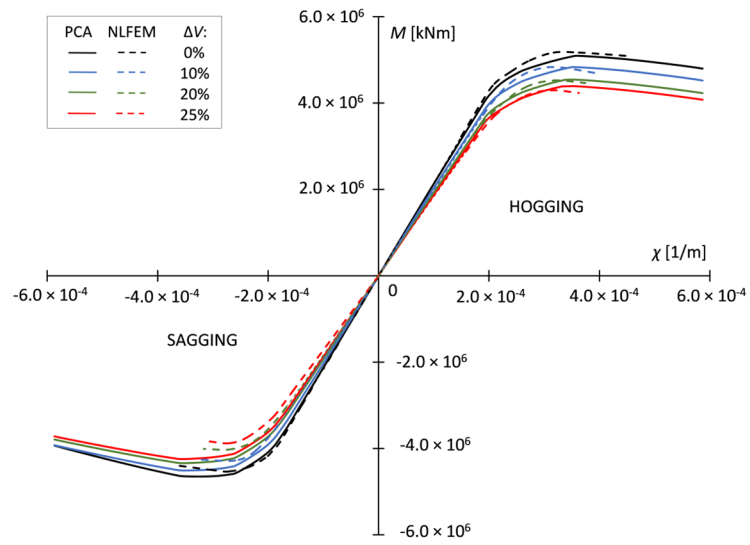
Figure 9. Case IV—intact and uniform corrosion-affected hull: bending moment vs. curvature.
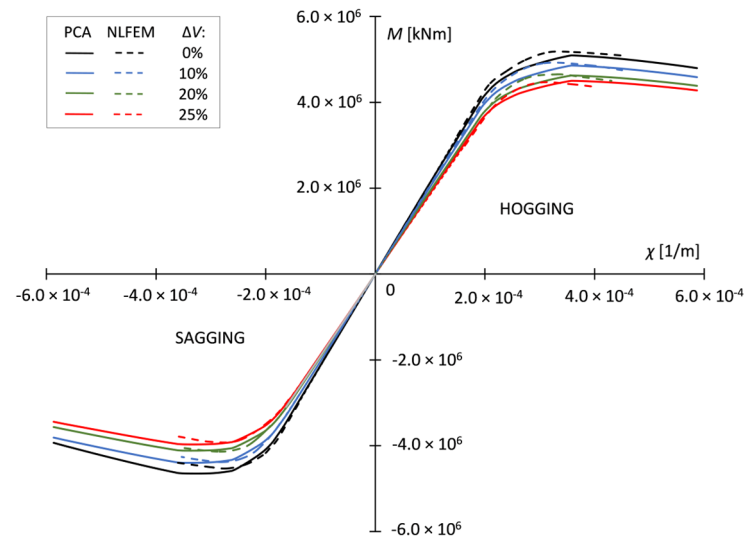

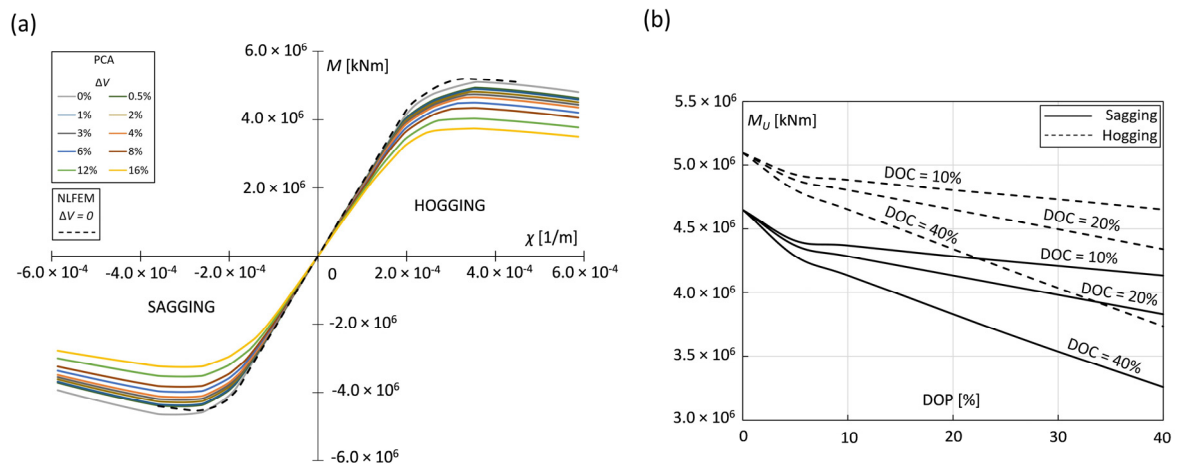**Figure 10.** Case V—intact and uniform corrosion-affected hull: bending moment vs. curvature.

Figure 11. Case I—intact and pitting corrosion-affected hull: (**a**) bending moment vs. curvature; (**b**) ultimate strength vs. DOP vs. DOC.
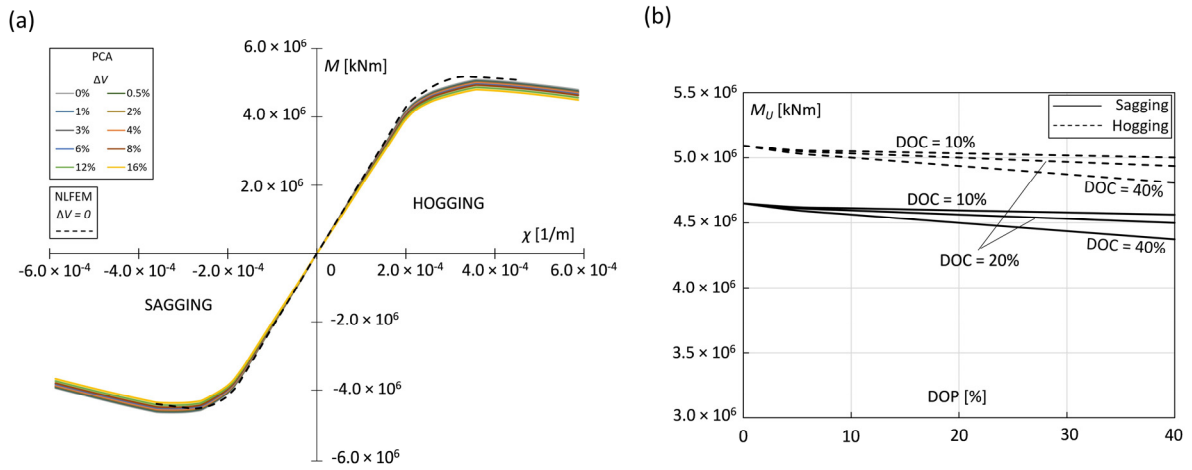
Figure 12. Case II—intact and pitting corrosion-affected hull: (**a**) bending moment vs. curvature; (**b**) ultimate strength vs. DOP vs. DOC.
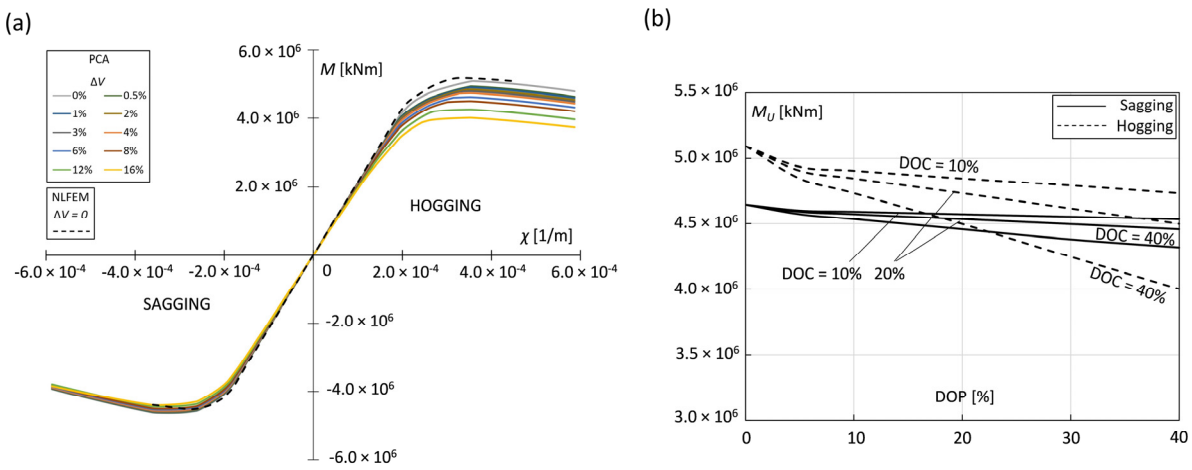

Figure 13. Case III—intact and pitting corrosion-affected hull: (**a**) bending moment vs. curvature; (**b**) ultimate strength vs. DOP vs. DOC.

Figure 14. Case IV—intact and pitting corrosion-affected hull: (**a**) bending moment vs. curvature; (**b**) ultimate strength vs. DOP vs. DOC.
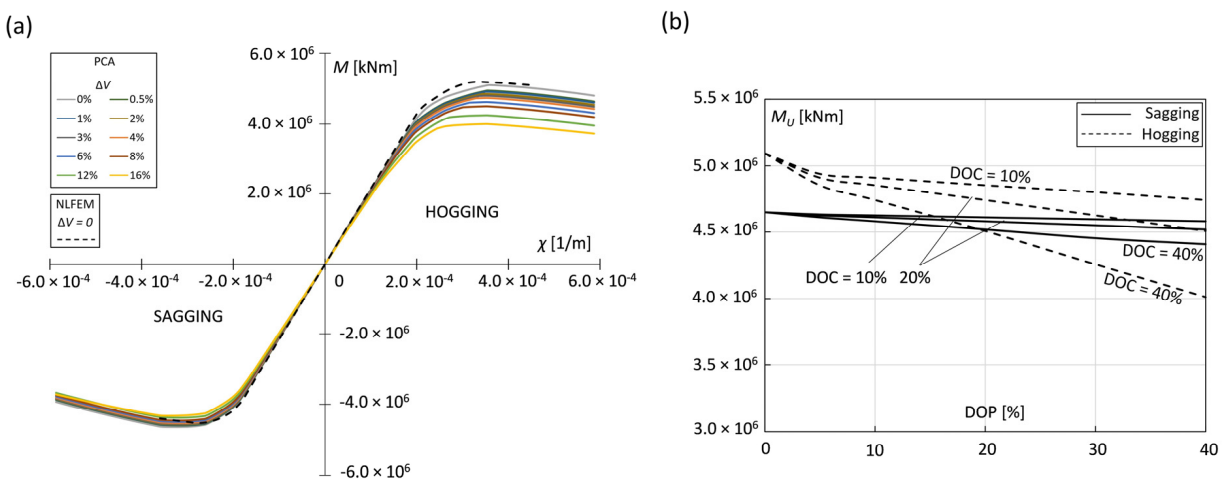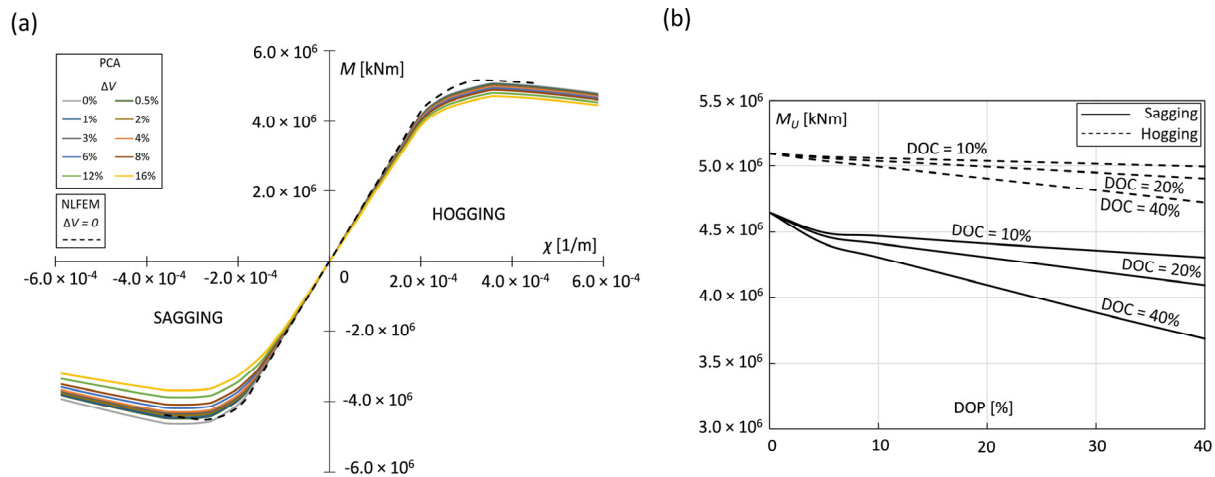
Figure 15. Case V—intact and pitting corrosion-affected hull: (**a**) bending moment vs. curvature; (**b**) ultimate strength vs. DOP vs. DOC.
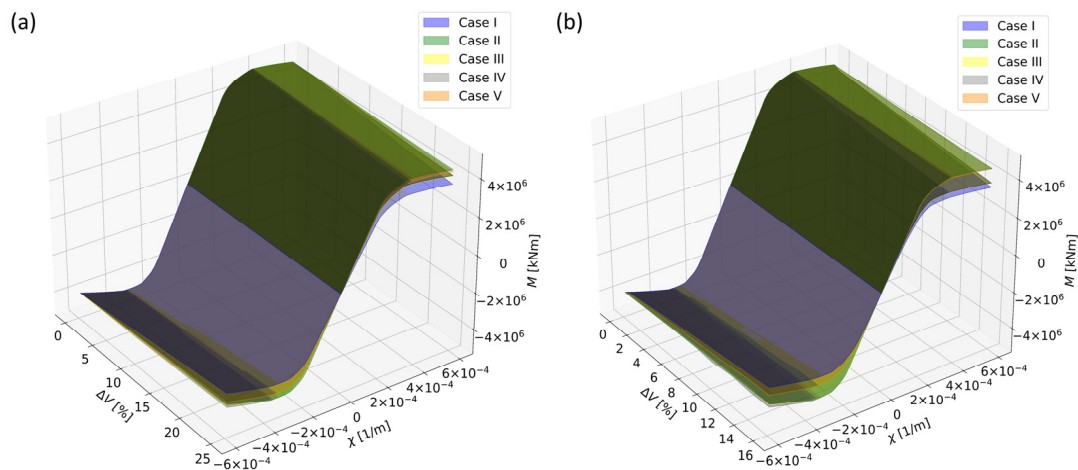

Figure 16. Bending moment vs. curvature 3D plots: (**a**) uniform corrosion cases; (**b**) pitting corrosion cases.

For the intact condition of the hull ($\Delta V = 0$), PCA and NLFEM provide good agreement. PCA delivers lower values, which are reached for larger curvatures. In hogging, the NLFEM results deviate from the PCA-calculated ultimate strength by 1.6% (PCA: 5.09×10^6 kNm, NLFEM: 5.17×10^6 kNm), and in sagging, by 2.6% (PCA: 4.65×10^6 kNm, NLFEM: 4.53×10^6 kNm).

In uniform corrosion scenarios, NLFEM differs from PCA ultimate strengths up to 9.5% (maximum difference is recorded for case III, with corrosion wastage 25%, in sagging condition). In fact, the largest differences in all cases are noted for 20% and 25% of wastage, in sagging, for cases II–IV. Generally, NLFEM-calculated diagrams follow the tendencies of their PCA counterparts.

The most extreme reduction in the ultimate strength due to uniform corrosion is found for case I. Namely, depending on the method used, 10% corrosion wastage reduces the ultimate strength of the intact hull by 7–10%, 20% by 19–25%, and 25% by 24–30%. In the rest of the cases, the reductions are much lower and similar to each other, with case II being the one with the lowest reductions for 10%, 20%, and 25% of the wastage, respectively, 3–6%, 6–12%, and 8–14%. The range between results for specific corrosion wastage is due to the methods considered (PCA or NLFEM) and whether the results were obtained for sagging or hogging.

Case I is, indeed, the most critical as it assumes that all elements experience corrosion at the same level. This can be considered as not realistic, so it is used here as a benchmarking case. Case II differs from case I only in the exclusion of stiffeners (longitudinals) from the corrosion. Nonetheless, case II delivers significantly lower reductions in the ultimate strength of the corroded hull, meaning that stiffeners carry a large portion of the total hull girder ultimate strength. Cases III–V include elements that mostly corrode in bulk carrier practice, including stiffener corrosion, and can be considered as more realistic. Their ultimate strength reductions vary between 3 and 7% for 10% wastage, 7 and 13% for 20% wastage, and 9 and 17% for 25% wastage. It can be concluded that uniform corrosion wastage affects the ultimate strength of the hull gradually, with respect to the amount of corrosion wastage presumed.

Pitting scenarios produce even larger discrepancies in the ultimate strength results than uniform corrosion does. Depending on the volume loss, the reductions in ultimate strength are from 0.41–5.16% (for $\Delta V = 0.5\%$) to 5.18–29.86% (for $\Delta V = 16\%$), depending on the cases considered. As for uniform corrosion, pitting corrosion in case II produces, overall, the lowest ultimate strength reductions compared to the intact hull: up to 5.6% for hogging and 6% for sagging (for $\Delta V = 16\%$). Furthermore, case I remains the most critical one for pitting, as the largest reductions were recorded for the most extreme presumed volume loss, for sagging and hogging, respectively, 26.6% and 29.9%. More realistic scenarios may include pitting corrosion with an amount of $\Delta V = 6\%$ (for instance, produced by DOP $\times$ DOC = 30% $\times$ 20%) for cases III–V. This delivers ultimate strength reductions between 2.18% and 9.71%. Sagging conditions give significantly larger ultimate strength reductions than hogging scenarios in case V, contrary to the trends in cases III and IV. The former includes corroded elements above the neutral axis (most distanced); thus, those elements tend to buckle even before the bottom elements yield. Cases III and IV perform in a different way as the majority of their elements are below the neutral axis. Although existing, such discrepancies between the sagging and hogging ultimate strength reductions were not found in uniform corrosion scenarios. Uniform corrosion delivers slightly more similar reductions in both of the bending responses. On the other hand, as in the uniform corrosion cases, in pitting, as the volume loss increases, the ultimate strength for all cases decreases almost proportionally. Ultimate strengths are extracted, and volume losses are separated into their products, DOP and DOC; hence, such dependencies are shown on pitting diagrams (right part of diagrams in Figures 11–15). There, one can obtain ultimate strength values based on assumed pitting and corrosion intensity degrees, rather than using volume loss inputs.

To summarize, when taking into account both uniform and pitting corrosion effects together, the scenario in which all elements of the hull experience corrosion (case I) is the one with the largest ultimate strength reductions, both in sagging and hogging. It is also the least realistic case. Contrary to this, the case in which the corrosion of the stiffeners is neglected (case II) provides the lowest reductions in ultimate strength, proving the importance of stiffeners in the overall ultimate strength of the hull. Ultimate strength reductions are almost gradual in all cases and scenarios, depending on the amount of material loss (thickness or volume) in both corrosion types. The thickness loss for element renewal is 15% to 25% [14], in general, according to the rules and regulations of classification societies. However, only in case I (completely corroded hull) were the ultimate strength reductions larger than material loss inputs. Although significant reductions exist, in other cases, the amount of ultimate strength reduction is lower than the values of material loss inputs.

Note that this hull is completely made of high-strength steels, which provide significantly higher yield and buckling critical stresses for single structural segments compared to traditional mild steels. Nonetheless, the final ultimate strength of the hull girder is still significantly affected by corrosion-induced degradation.

Note that there is a lack of experiments regarding the ultimate strength of hull girders, so these results cannot be verified in that context. According to the best of the authors'

knowledge, almost all experimental data are related to the examinations of collapses of particular segments; see, for instance, studies on platings in [47,48] and on stiffeners with attached platings in [49,50]. Thus, here, we aimed to synthetize the influences of these particular segment-to-segment collapses for the ultimate strength assessment of large and complex structures additionally subjected to corrosion degradation.

5. Conclusions

In this study, we used a case study of a bulk carrier hull completely made of high-strength steel to perform ultimate strength assessments in intact and corroded conditions for five different cases of affected hull elements. Consequently, the following conclusions are presented:

- NLFEM- and PCA-calculated hull girder ultimate strengths for elements impacted by uniform corrosion differ by up to 9.5% (maximum is for 25% of wastage in sagging);
- The ultimate strength of the hull gradually reduces as the corrosion losses increase (almost linearly for all cases), considering the percentage of the corrosion wastage (uniform corrosion) and volume loss (pitting corrosion);
- Stiffeners have a large influence on the ultimate strength of the hull; thus, their corrosion should not be neglected in ultimate strength assessment scenarios;
- The largest ultimate strength reductions (up to 30%) are recorded for the case in which all elements experience corrosion, for both uniform corrosion, which considers 25% of wastage, and pitting, which includes $\Delta V = 16\%$;
- In more realistic scenarios of the corrosion severity (10% wastage due to uniform corrosion, and $\Delta V = 6\%$ for pitting corrosion) and for cases in which the corrosion occurred on parts of the hull (cases III-V), the ultimate strength reductions were recorded as 3–7% (uniform) and 2.18–9.71% (pitting).

This study shows the importance of incorporating age-related phenomena such us corrosion in ultimate strength calculations, as they appear to have a significant effect on the ultimate capacity of hull girders to carry the vertical bending moment. Industry practice, which is to assess the structural design of the ship as intact rather than corroded, should be updated, as ships navigate with some elements experiencing a notable level of corrosion. Coupled with other unpredicted events and loadings ship can encounter, corrosion can speed up the progressive collapse of the hull, and this should not be overlooked.

Author Contributions: N.M.: Conceptualization, data curation, formal analysis, funding acquisition, methodology, project administration, software, supervision, visualization, writing—original draft, writing—review and editing. N.I.: Conceptualization, data curation, formal analysis, investigation, software, validation, visualization, writing—review and editing. M.K.: data curation, methodology, funding acquisition, resources, writing—review and editing. Š.I.: Funding acquisition, methodology, resources, writing—review and editing. A.P.: Funding acquisition, methodology, resources, writing—review and editing. All authors have read and agreed to the published version of the manuscript.

Institutional Review Board Statement: Not applicable.

Informed Consent Statement: Not applicable.

Data Availability Statement: Data are contained within the article.

Conflicts of Interest: The authors declare no conflicts of interest.

References

1. Hughes, O.F.; Paik, J.K. *Ship Structural Analysis and Design*; SNAME: Alexandria, VA, USA, 2010.
2. Paik, J.K. *Ultimate Limit State Analysis and Design of Plated Structures*; John Wiley & Sons Ltd.: Hoboken, NJ, USA, 2018.
3. Lloyd's Register. *Rules and Regulations for the Classification of Ships*; Lloyd's Register: London, UK, 2022.
4. Bureau Veritas. *Rules for the Classification of Steel Ships, NR467*; Bureau Veritas: Paris, France, 2023.

5. Yao, T.; Fujikubo, M. *Buckling and Ultimate Strength of Ship and Ship-Like Floating Structures*; Elsevier: Amsterdam, The Netherlands, 2016.

6. BMA. *Report of the Investigation into the Sinking of the "MOL Comfort" in the Indian Ocean*; The Bahamas Maritime Authority: London, UK, 2015.

7. Freight News. Available online: https://www.freightnews.co.za/article/questions-raised-over-carrier-sinking-within-sight-land-and-two-other-vessels (accessed on 15 January 2024).

8. Sumi, Y. Structural safety of ships developed by lessons learned from the 100-year history of break-in-two accidents. *Mar. Struct.* **2019**, *64*, 481–491. [CrossRef]

9. International Maritime Organization. *Adoption of the International Goal-Based Ship Construction Standards for Bulk Carriers and Oil Tankers, MSC.287(87)*; International Maritime Organization: London, UK, 2010.

10. International Association of Classification Societies. *Common Structural Rules for Bulk Carriers and Oil Tankers (CSR-H)*; International Association of Classification Societies: London, UK, 2014. Available online: https://iacs.org.uk/resolutions/common-structural-rules/previous-csr (accessed on 20 January 2024).

11. International Association of Classification Societies. *Common Structural Rules for Bulk Carriers and Oil Tankers*; International Association of Classification Societies: London, UK, 2023. Available online: https://iacs.org.uk/resolutions/common-structural-rules/csr-for-bulk-carriers-and-oil-tankers (accessed on 20 January 2024).

12. International Ship and Offshore Structures Congress. Ultimate Strength Committee III.1. In Proceedings of the 20th International Ship and Offshore Structures Congress—ISSC 2018, Liege, Belgium; Amsterdam, The Netherlands, 9–14 September 2018. Available online: https://ebooks.iospress.nl (accessed on 25 January 2024).

13. Ivošević, Š.; Kovač, N.; Momčilović, N.; Vukelić, G. Evaluation of the corrosion depth of double bottom longitudinal girder on aging bulk carriers. *J. Mar. Sci. Eng.* **2022**, *10*, 1425. [CrossRef]

14. Det Norske Veritas. *Allowable Thickness Diminution for Hull Structure*; Det Norske Veritas: Oslo, Norway, 2020.

15. Jurišić, P.; Parunov, J.; Garbatov, Y. Aging effects on ship structural integrity. *Brodogradnja/Shipbuilding* **2017**, *68*, 2. [CrossRef]

16. Woloszyk, K.; Goerlandt, F.; Montewka, J. A methodology for ultimate strength assessment of ship hull girder accounting for enhanced corrosion degradation modelling. *Mar. Struct.* **2023**, *93*, 103530. [CrossRef]

17. Andrić, J.; Kitarović, S.; Bičak, M. IACS Incremental—Iterative method in progressive collapse analysis of various hull girder structures. *Brodogradnja/Shipbuilding* **2014**, *65*, 65–78.

18. Kitarović, S.; Andrić, J.; Pirić, K. Hull girder progressive collapse analysis using IACS prescribed and NLFEM derived load-end shortening curves. *Brodogradnja/Shipbuilding* **2016**, *67*, 115–128. [CrossRef]

19. Olmez, H.; Bayraktarkatal, E. Effects of key factors on hull girder ultimate strength estimation by progressive collapse calculations. *Lat. Am. J. Solids Struct.* **2016**, *13*, 2371–2392. [CrossRef]

20. Tekgoz, M.; Garbatov, Y.; Guedes Soares, C. Strength assessment of an intact and damaged container ship subjected to asymmetrical bending loadings. *Mar. Struct.* **2018**, *58*, 172–198. [CrossRef]

21. Kuznecovs, A.; Ringsberg, J.W.; Johnson, E.; Yamada, Y. Ultimate limit state analysis of a double-hull tanker subjected to biaxial bending in intact and collision-damaged conditions. *Ocean Eng.* **2020**, *209*, 107519. [CrossRef]

22. Alfred Mohammed, E.; Benson, S.D.; Hirdaris, S.E.; Dow, R.S. Design safety margin of a 10,000 TEU container ship through ultimate hull girder load combination analysis. *Mar. Struct.* **2016**, *46*, 78–101. [CrossRef]

23. Jagite, G.; Bigot, F. Numerical investigation of the hull girder ultimate strength under realistic cyclic loading derived from long-term hydroelastic analysis. *Ships Offshore Struct.* **2022**, *18*, 515–528. [CrossRef]

24. Li, S.; Kim, D.K. A comparison of numerical methods for damage index based residual ultimate limit state assessment of grounded ship hulls. *Thin-Walled Struct.* **2022**, *172*, 108854. [CrossRef]

25. International Ship and Offshore Structures Congress. Ultimate Strength Committee III.1. In Proceedings of the 21st International Ship and Offshore Structures Congress—ISSC 2022, Vancouver, BC, Canada, 11–15 September 2022. [CrossRef]

26. Nouri, Z.; Khedmati, M.R. Progressive collapse analysis of an FPSO vessel hull girder under vertical bending considering different corrosion models. *J. Mar. Sci. Appl.* **2020**, *19*, 674–692. [CrossRef]

27. Georgiadis, D.; Samuelides, M. A methodology for the reassessment of hull-girder ultimate strength of a VLCC tanker based on corrosion model updating. *Ship Offshore Struct.* **2019**, *14*, 270–280. [CrossRef]

28. Vu Van, T.; Yang, P. Effect of corrosion on the ship hull of a double hull very large crude oil carrier. *J. Mar. Sci. Appl.* **2017**, *16*, 334–343. [CrossRef]

29. Vu Van, T.; Tuan Dong, D. Hull girder ultimate strength assessment considering local corrosion. *J. Mar. Sci. Appl.* **2020**, *19*, 693–704. [CrossRef]

30. Lampe, J.; Hamann, R. Probabilistic model for corrosion degradation of tanker and bulk carrier. *Mar. Struct.* **2018**, *61*, 309–325. [CrossRef]

31. Momčilović, N.; Ilić, N.; Kalajdžić, M.; Ivošević, Š.; Petrović, A. Pitting and uniform corrosion effects on ultimate strength of a bulk carrier. Second International Symposium on Risk Analysis and Safety of Complex Structures and Components (IRAS 2023). *Procedia Struct. Integr.* **2023**, *48*, 12–18. [CrossRef]

32. Piscopo, V.; Scamardella, A. Incidence of Pitting Corrosion Wastage on the Hull Girder Ultimate Strength. *J. Mar. Sci. Appl.* **2021**, *20*, 477–490. [CrossRef]

33. Piscopo, V.; Scamardella, A. Towards a unified formulation for the ultimate strength assessment of uncorroded and pitted platings under uniaxial compression. *Ocean Eng.* **2018**, *169*, 70–86. [CrossRef]

34. Piscopo, V.; Scamardella, A. Ultimate strength assessment of intact and pitted platings under biaxial compression. *Eng. Struct.* **2020**, *204*, 110079. [CrossRef]

35. Woloszyk, K.; Kahsin, M.; Garbatov, Y. Numerical assessment of ultimate strength of severe corroded stiffened plates. *Eng. Struct.* **2018**, *168*, 346–354. [CrossRef]

36. Feng, L.; Hu, L.; Chen, X.; Shi, H. A parametric study on effects of pitting corrosion on stiffened panels' ultimate strength. *Int. J. Nav. Arch. Ocean Eng.* **2020**, *12*, 699–710. [CrossRef]

37. Anyfantis, K.N.; Pantazopoulou, S.; Papanikolaou, N. Generalized probabilistic response surfaces for the buckling strength assessment of stiffened panels. *Thin-Walled Struct.* **2023**, *189*, 110860. [CrossRef]

38. Hanif, M.; Imaduddin, M.; Adiputra, R.; Prabowo, A.R.; Yamada, Y.; Firdaus, N. Assessment of the ultimate strength of stiffened panels of ships considering uncertainties in geometrical aspects: Finite element approach and simplified formula. *Ocean Eng.* **2023**, *286*, 115522. [CrossRef]

39. Tekgoz, M.; Garbatov, Y. Collapse strength of intact ship structures. *J. Mar. Sci. Eng.* **2021**, *9*, 1079. [CrossRef]

40. Tekgoz, M.; Garbatov, Y.; Guedes Soares, C. Review of ultimate strength assessment of ageing and damaged ship structures. *J. Mar. Sci. Appl.* **2020**, *19*, 512–533. [CrossRef]

41. Equasis. *The 2021 World Merchant Fleet Statistics from Equasis*; Equasis: Lisbon, Portugal, 2021.

42. UNCTAD. *Review of Maritime Transport 2022*; UNCTAD: Geneva, Switzerland, 2022.

43. International Association of Classification Societies. *No.47 Shipbuilding and Repair Quality Standard*; International Association of Classification Societies: London, UK, 2012.

44. Smith, C.S. Influence of local compressive failure on ultimate longitudinal strength of a ship's hull. In Proceedings of the International Symposium on Practical Design in Shipbuilding (PRADS), Tokyo, Japan, 18–20 October 1977; pp. 73–79.

45. Paik, J.K.; Kim, D.K. Advanced method for the development of an empirical model to predict time-dependent corrosion wastage. *Corros. Sci.* **2012**, *63*, 51–59. [CrossRef]

46. Paik, J.K.; Lee, J.M.; Park, Y.I.; Hwang, J.S.; Kim, C.W. Time-variant ultimate longitudinal strength of corroded bulk carriers. *Marine Struct.* **2003**, *16*, 567–600. [CrossRef]

47. Wang, R.H.; Lin, S. On the effect of pit shape on pitted plates, Part I: Tensile behavior due to artificial corrosion pits. *Ocean Eng.* **2021**, *236*, 108754. [CrossRef]

48. Garbatov, Y.; Tekgoz, M.; Guedes Soares, C. Experimental and numerical strength assessment of stiffened plates subjected to severe non-uniform corrosion degradation and compressive load. *Ships Offshore Struct.* **2017**, *12*, 461–473. [CrossRef]

49. Shi, X.H.; Zhang, J.; Guedes Soares, C. Numerical assessment of experiments on the ultimate strength of stiffened panels with pitting corrosion under compression. *Thin-Walled Struct.* **2018**, *133*, 52–70. [CrossRef]

50. Zhang, J.; Shi, X.H.; Guedes Soares, C. Experimental analysis of residual ultimate strength of stiffened panels with pitting corrosion under compression. *Thin-Walled Struct.* **2017**, *114*, 39–51. [CrossRef]